

Automatic estimation of volcanic ash plume height using WorldView-2 imagery

David McLaren^a, David R. Thompson, Ashley G. Davies^a,
Magnus T. Gudmundsson^b, Steve Chien^{a*}

^aJet Propulsion Laboratory, California Institute of Technology,
4800 Oak Grove Drive, Pasadena, CA USA 91109-8099

^bInstitute of Earth Sciences, University of Iceland, Sturlugata 7, 101 Reykjavik, Iceland.

ABSTRACT

We explore the use of machine learning, computer vision, and pattern recognition techniques to automatically identify volcanic ash plumes and plume shadows, in WorldView-2 imagery. Using information of the relative position of the sun and spacecraft and terrain information in the form of a digital elevation map, classification, the height of the ash plume can also be inferred. We present the results from applying this approach to six scenes acquired on two separate days in April and May of 2010 of the Eyjafjallajökull eruption in Iceland. These results show rough agreement with ash plume height estimates from visual and radar based measurements.

Keywords: sensorweb, volcanoes, volcanic ash, machine learning, computer vision, pattern recognition, WorldView-2, multispectral

1. INTRODUCTION

Rapid growth in the quantity and quality of commercial remote sensing can enable greatly enhanced environmental monitoring. Recently launched satellites make available extremely high spatial resolution multispectral imagery. However, in order to provide high-spatial-resolution data, these satellites are point-and-shoot. Generally, targeted observations must be requested and scheduled well in advance of target overflight.

“Sensorweb” operations is a concept of operations in which data from multiple satellites are assimilated to better track an event or environmental phenomenon of significance. In the sensorweb concept, data are assimilated from satellites and other sources, and used to: (a) model and track the phenomena of interest, and (b) drive future targeting. The key is that the modeling and tracking provide more timely and detailed information than would be available from purely prescheduled observations. The desire for detailed information generally favors the highest spatial resolution data that is available. The desire to provide timely information means that ideally the data acquisition, processing, and modeling is done automatically. If the future spacecraft targeting process can be automated (e.g., [Chien et al. 2011]), subsequent data can be obtained at the highest temporal resolution. More precise modeling of the ongoing “interesting” process is enabled.

WorldView-2, a satellite launched in 2009 and operated by DigitalGlobe, has extremely high-spatial resolution (2 m / pixel) combined with a multispectral (8 bands at 0.45 – 1.05 μm) capability. Using Control Moment Gyro (CMG) technology, WorldView-2 is extremely agile and can acquire multiple images of a target during a single overflight. In this paper we explore the use of WorldView-2 in a sensorweb to track volcanic activity around the world.

* Contact author: steve.chien@jpl.nasa.gov, contact any JPL author at: firstname.lastname@jpl.nasa.gov

Appears as paper 8390-52, Proceedings of SPIE Algorithms and Technologies for Multispectral, Hyperspectral, and Ultraspectral Imagery XVIII, Baltimore, MD, April 2012.

Hundreds of millions of people live within high-risk volcano hazard zones [Ewert & Harpel, 2004]. The recent (2010) eruptions of the Eyjafjallajökull volcano in Iceland highlighted the impact to the global economy of a single volcano, disrupting air traffic across the Atlantic and Europe for a sustained period of time. Economic costs were in the billions of USD with direct impact to air travel being estimated at \$1.7B USD [BBC].

Plume measurements, including height, volume, density, lateral extent, and rise (ejection) velocity, are critical to volcano monitoring because of the direct impact of volcanic ash on transportation, agriculture, and human health. Plume height measurement in particular provides valuable data as to the strength and mechanisms of the volcanic eruption itself, allowing estimation of the volumetric eruption rate, a critical parameter for estimating the volumes of ash ejected into the atmosphere.

This paper describes how high-spatial-resolution, multispectral WorldView-2 data can be used to automatically detect and map volcanic plumes. We describe how this plume map can be combined with sun illumination geometry information to yield an automatic lower-bound measurement of plume height. We apply these algorithms to two sets of WorldView-2 images of the Eyjafjallajökull eruption of 2010 and compare the automatically-derived estimates to externally-derived estimates of plume height.

2. AUTOMATED VOLCANIC ASH DETECTION IN WORLDVIEW-2 DATA

2.1 WorldView-2 data, Radiometric and atmospheric correction

Our initial study used 10 WorldView-2 images acquired of the Eyjafjallajökull volcano in April and May of 2010. Of these 10 images, 2 contained no plume and 2 contained plume, but no plume shadow. As the presence of a plume shadow is needed to estimate plume height, our study therefore focused on the 6 remaining images.

We first converted these images to top-of-atmosphere reflectance [DigitalGlobe] before subsequent processing. However, this method still left considerable variance in brightness that hampered across-image analysis. We later switched to taking images not corrected to top-of-atmosphere reflectance and instead enhanced the contrast of each image using histogram equalization [Histogram]. We trained and ran our classifier on the histogram-equalized images. We oriented the resulting classification maps so that solar illumination came from the bottom of the image, using solar angles recorded in the observation metadata. Figure 1 shows a sample input image (at left) and a histogram equalized image (at right).

2.2 Machine learning approach

We employ an image analysis technique method previously developed for in situ surface imagery. TextureCam [Thompson et al. 2012] is a framework and library of image processing and classification techniques intended for integration into a “smart” instrument. A machine learning strategy exploits manually labeled image regions to train a random forest classifier [Breiman 2001, Shotton et al. 2008]. We train this system to recognize the statistics of local image patches corresponding to: airborne ash plume, shadow, and other (including land, water, and ice). The learned classifier is intended to generalize to new scenes under different terrain and lighting conditions. It ascribes a probabilistic surface classification to each pixel that incorporates cues learned from multispectral intensity, local texture, local pixel statistics, and other image data.

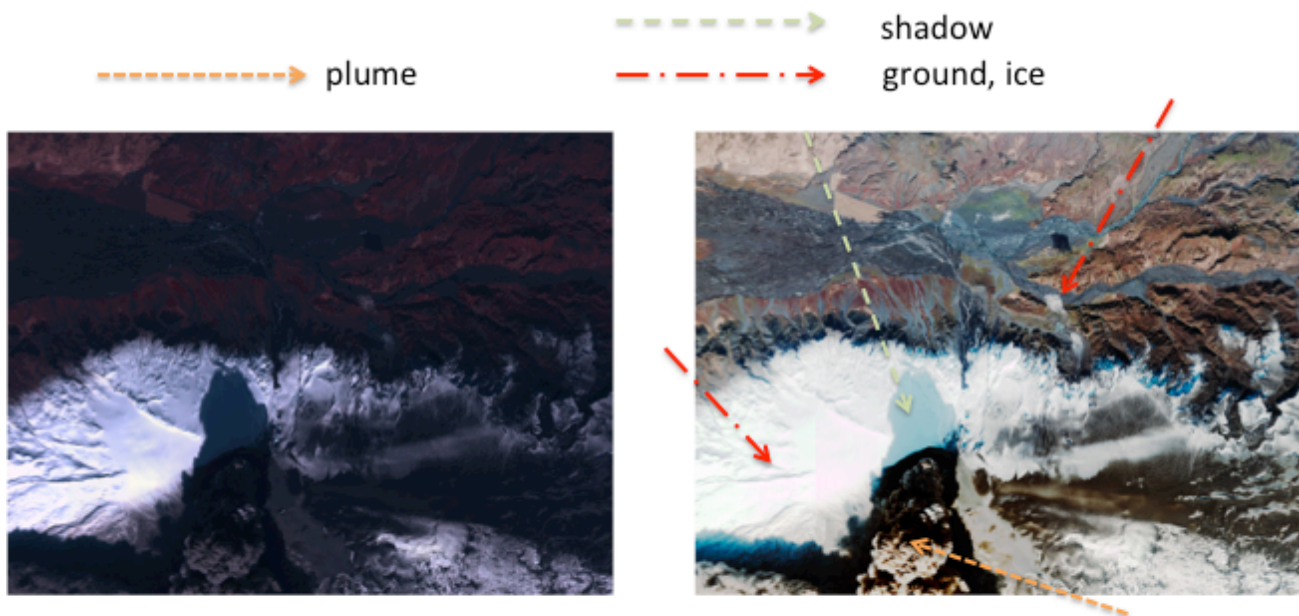


Figure 1: Worldview-2 Image (L) and Histogram-equalized WV-2 image (R) of Eyfjallajokull eruption, April 2010. Regions of plume, shadow, ground, and ice indicated.

In order to apply TextureCam to the WorldView-2 volcanic plume classification task we defined several input features. First, we specified all ratios of the 8 spectral bands available in WorldView-2 data, thus providing 28 features. The resultant decision trees derive the classification map shown in Figure 2, created by running the learned classifier on the image in Figure 1. Figure 2 (left) shows the probabilistic surface classification for the plume class, Figure 2 (middle) shows the probabilistic classification for the shadow class, and Figure 2 (right) shows the classification map for the other class.

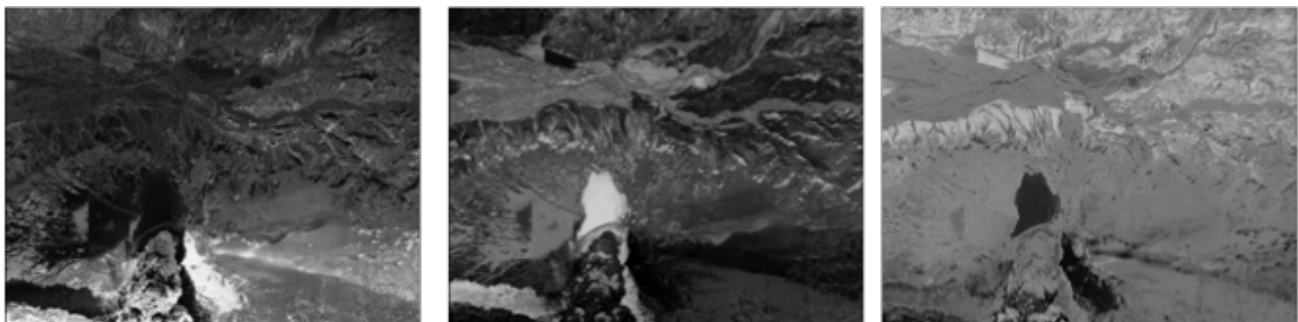


Figure 2: Probability maps derived from TextureCam (lighter = higher probability) for plume (left), shadow (center), other/land (right)

Typical decision tree classifiers can provide a single label for each pixel based on the Maximum A Posteriori (MAP) classification - the most probable class of each datapoint. This label is based on image cues, but it is also influenced by the abundance of each class in the training images. For this reason it may not be the optimal solution for the specific accuracy requirements of the task. Consequently users often

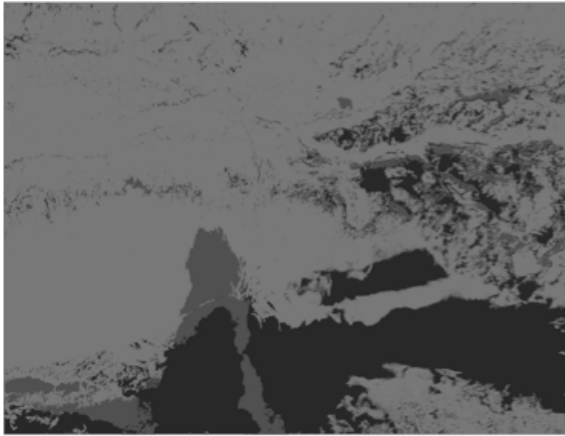


Figure 3: Integrated classification map where black = plume, grey = shadow, light = background/land.

modify classification thresholds to favor one class or another. Our analysis uses classification thresholds that optimize the end goal of accurately estimating the anti-sunward edge of the ash plume and the extent of anti-sunward shadow adjacent to the ash. In order to further enhance accuracy we subsequently smooth and filter the classification map and apply segmentation techniques to sharpen the ash cloud boundary. Figure 3 shows the classification map for the image shown in Figure 1.

One of the key features of our interpretation method is that it should be scene, target, and illumination invariant. We trained the method on one image and applied it to a set of 5 different images (a total of 6 images in all). While all of the images were of the same target (the Eyjafjallajökull volcano) the images span two days and a range of viewing angles.

Figure 4 shows the histogram equalized image (left) and classification map (right) on a separate Eyjafjallajökull observation acquired on a different day.

Our detection method is able to classify large areas of ash plume and shadow but experiences a number of difficulties:

1. *Dark portions of the ash plume are classified as shadows.* Indeed, due to the billowing nature of the ash plume, there are often large shadowed areas within the ash plume. Additionally, stair-step

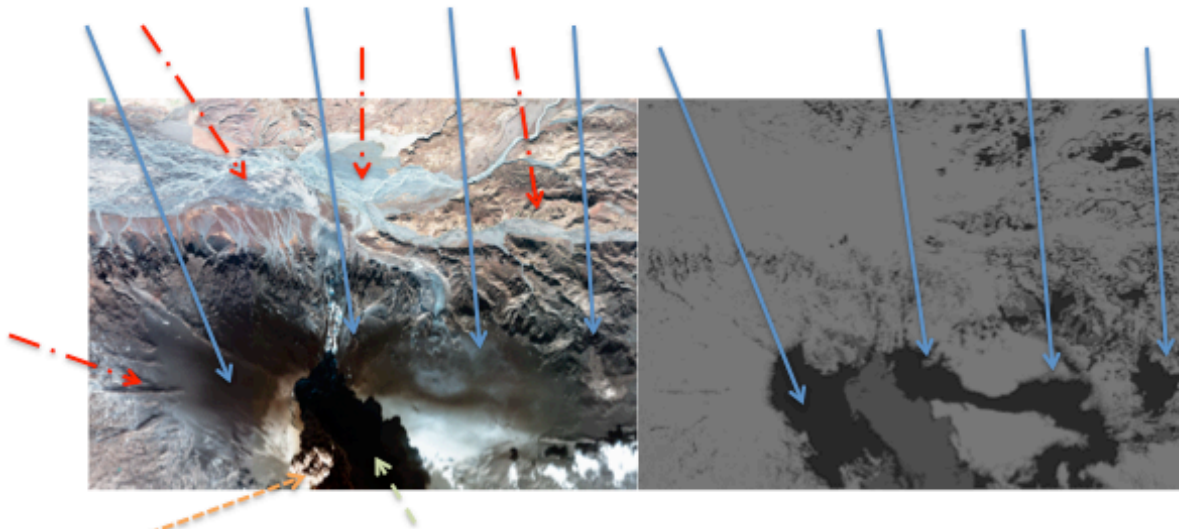


Figure 4: Image highlighting correct and incorrect classifications
 Left – histogram equalized worldview-2 image
 Right – classification map: black = plume, grey = shadow, light = land

structure in the ash plume can also create large shadowed areas within the ash plume. We attempt to address this issue by smoothing the classification map to remove these smaller shadows out of the final ash plume classified region.

2. *Large areas of land are classified as ash plume.* Because our method relies on spectral features, land that may be covered with ash or spectrally similar materials may be misclassified as ash in a plume. We do not process these areas out but, because we are searching for shadow regions to the anti sunward side of ash plume regions, these types of misclassifications are unlikely to harm our calculations.
3. *Shadows may occur due to land features.* Because these areas are likely to be small and not have large ash regions to the sunward direction, they do not harm our calculations.
4. *Plume shadow is partially or fully out of frame.* Alternatively, the shadow may be in the image frame, but the plume is not. In general we discard plume and shadow estimates that run into the edge of the image.

Figure 4 shows a histogram-equalized image and class map indicating some of the classification difficulties. In particular, blue arrows highlight the difficulties in spectral based discrimination between ash plume and certain ground surfaces (in this case ash on the ground).

Once the ash cloud and shadow has been identified, the image can be processed to estimate shadow length and therefore plume height above sea level [Prata & Grant 2001]. This algorithm works by finding line segments that run from sunward to anti-sunward direction that consist of a region of ash followed by a region of shadow. Each of these shadow measurements must then be corrected for:

1. relative position of the spacecraft
2. relative position of the sun
3. relative ground elevation of the shadow point

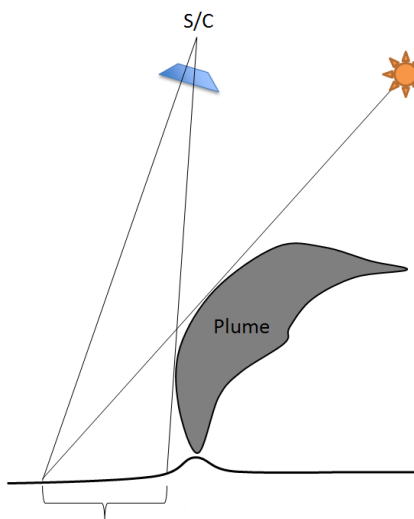


Figure 5: Visible shadow lower-bounds plume height

to produce the estimate for the height of the plume edge above sea level. We utilize the ASTER GDEM2 digital elevation map (30 m horizontal spacing, 1 m vertical spacing) to correct for terrain effects.

One issue is that even assuming a perfect classification, our method produces an underestimate of plume because the plume possibly has a complex stair step structure rather than a single upward then windward structure. In order to address this difficulty we select the longest shadow rays that trace from large areas of plume, and compute plume heights corresponding to these rays. We then compute the mean and standard deviation of the top quartile of plume height estimates, and discard all plume height estimates farther than two standard deviations from this mean. The remaining plumes constitute our final sample for analysis. For our best estimate, we report the mean of the plume heights in this sample. We also report the 20-80 percentile range of the remaining plume heights as an uncertainty estimate.

3. PLUME HEIGHT ESTIMATION FOR THE 2010 EYJAFJALLAJÖKULL ERUPTION

3.1 Results

We took the trained ash/shadow/background classifier from a single image from 17 April 2010 WorldView-2 overflight of the Eyjafjallajökull volcano and applied it that same image and to another 5 WorldView-2 images of the Eyjafjallajökull volcano. In all the images were acquired both 17 April and 11 May 2010 with a moderate range of lighting conditions with widely varying plumes. Table 1 below shows the estimated plume height ranges derived using the above shadow-based algorithms for each of the images. Table 1 also shows the independent visual and radar measurements [Arason et al. 2011] estimating the plume heights on the same days in question. The data shows reasonable agreement between the plume height estimated from WorldView-2 data and from other sources.

Image	Plume height estimate (in km above sea level)				
	WorldView-2 Shadow-based Estimates			Estimates from [Arason et al. 2011]	
	# of samples	Best estimate (mean) (in km)	20 th - 80 th %-ile Range (in km)	Visual Estimate	Radar Estimate
17 April 2010	290	2.66	2.52-2.97	2.3-5.5km (Figure 9)	4.8-8.5km (Figure 9)
17 April 2010	199	3.57	3.51-3.64		
17 April 2010	585	3.06	2.94-3.15		
17 April 2010	8	4.35	4.35-4.36		
11 May 2010	12	3.02	3.02-3.03	3.8-4.4 km, mean=4.3km (Figure 10)	3.6-4.9 km, mean = 4.3km (Figure 10)
11 May 2010	154	4.58	4.47-4.67		

Table 1: Comparison of plume height estimates from WorldView-2 shadow based derivation to visual and radar measurements from [Arason et al. 2011] for WorldView-2 scenes from 17 April 2010 and 11 May 2010.

3.2 Related and Future Work

Extensive work with the MISR instrument has retrieved aerosol, plume, and cloud heights [Moroney et al. 2002, Kahn et al. 2007]. MISR is also a multi-look instrument, so the altitude of plumes and other aerosols can be inferred by relative positioning and stereo reconstruction. With these techniques in mind, we will further explore the use of landmark/feature tracking in the hyper-stereo WorldView-2 image sequences to estimate plume velocity (e.g., we have one 4-scene sequence and one 2-scene sequence of images).

The classifier described here uses a single training image, but additional training data are likely to enhance performance by exposing the learning system to different terrain, plume, and imaging conditions. We also have acquired additional WorldView-2 imagery and other multispectral imagery (IKONOS and GeoEye) of a number of volcanic events in the 2011 timeframe, including Grimsvotn (Iceland), Katla (Iceland), Puyehue-Cordon Caulle (Chile), Merapi (Indonesia), and Etna (Italy). We would like to extend these techniques to additional sensors, episodes, and sites towards our eventual goal of a worldwide volcano monitoring system that would provide ash related data on demand [Chien et al. 2005, 2011].

4. CONCLUSIONS

We have described a machine-learning approach to automatic plume height estimation from high resolution multispectral data from the WorldView-2 satellite. In this approach, histogram-equalized, contrast-enhanced imagery is used in concert with a decision forest machine learning approach to identify regions of volcanic ash plume, shadow, and background. Knowledge of the relative position of the sun and digital elevation information are combined to produce a set of estimates for the altitude of the plume above sea level. We present early results of application of this approach to a small set of images from the Eyjafjallajökull eruption of April-May 2010. These results show reasonable agreement with independent visual and radar-based measurements of the plume. We hope to eventually extend these methods to other volcanic eruptions, making use of other satellite sensors.

5. ACKNOWLEDGEMENTS

Portions of this work were performed by the Jet Propulsion Laboratory, California Institute of Technology, under contract from the National Aeronautics and Space Administration.

REFERENCES

- [1] P. Arason, G.N. Petersen and H. Björnsson, “Observations of the altitude of the volcanic plume during the eruption of Eyjafjallajökull, April-May 2010,” *Earth System Sciences Data*, 3, 9-17 (2011).
- [2] BBC News, “Flight disruptions cost airlines \$1.7bn, says IATA,” retrieved on 13 March 2012, <http://news.bbc.co.uk/2/hi/business/8634147.stm> (2012).
- [3] L. Breiman, *Machine learning* 45(1):5 (2001).
- [4] S. Chien, B. Cichy, A. Davies, D. Tran, G. Rabideau, R. Castano, R. Sherwood, D. Mandl, S. Frye, S. Shulman, J. Jones, S. Grosvenor, “An Autonomous Earth Observing Sensorweb,” *IEEE Intelligent Systems*, May-June 2005, pp. 16-24 (2005).
- [5] S. Chien, A. Davies, J. Doubleday, D. Tran, S. Jones, E. Kjartansson, K. Vogfjord, M. Gudmundsson, T. Thordarson, D. Mandl, “Integrating Multiple Space and Ground Sensors to Track Volcanic Activity,” 34th International Symposium on Remote Sensing of Environment, April 2011, Sydney, Australia (2011).
- [6] A. G. Davies, S. Chien, V. Baker, T. Doggett, J. Dohm, R. Greeley, F. Ip, R. Castaño, B. Cichy, G. Rabideau, D. Tran and R. Sherwood, “Monitoring Active Volcanism with the Autonomous Sciencecraft Experiment on EO-1,” *Remote Sensing of the Environment*, 101, no. 4, 427-446 (2006).
- [7] A. G. Davies, J. Calkins, L. Scharenbroich, R. Vaughan, R. Wright, P. Kyle, R. Castano, S. Chien, and D. Tran, “Multi-Instrument Remote and In Situ Observations of the Erebus Volcano (Antarctica) Lava Lake in 2005: a Comparison with the Pele Lava Lake on the Jovian Moon Io,” *Journal of Volcanology and Geothermal Research*, (2008).
- [8] DigitalGlobe, *worldview2.digitalglobe.com*, (2012).
- [9] DigitalGlobe, “Radiometric Use of WorldView-2 Imagery.” Technical Note. Accessed March 2, 2012. http://www.digitalglobe.com/downloads/Radiometric_Use_of_WorldView-2_Imagery.pdf, (2012).
- [10] J. W. Ewert and C. J. Harpel, “In harm’s way: population and volcanic risk,” *Geotimes*, 49, no. 4, 14-17 (2004).
- [11] Wikipedia, “Wikipedia: Histogram Equalization,” http://en.wikipedia.org/wiki/Histogram_equalization, retrieved 13 March (2012).
- [12] Kahn, R. A., W.-H. Li, C. Moroney, D. J. Diner, J. V. Martonchik, and E. Fishbein, Aerosol source plume physical characteristics from space-based multiangle imaging, *J. Geophys. Research*, 112, D11205 (2007).

Appears as paper 8390-52, Proceedings of SPIE Algorithms and Technologies for Multispectral, Hyperspectral, and Ultraspectral Imagery XVIII, Baltimore, MD, April 2012.

- [13] Machine Learning and Instrument Autonomy (MLIA) Group, Jet Propulsion Laboratory, "PixelLearn Users Guide," mlia.jpl.nasa.gov, (2008).
- [14] C. Moroney, R. Davies, J.-P. Muller,, "Operational retrieval of cloud-top heights using MISR data," *Geoscience and Remote Sensing, IEEE Transactions on* , vol.40, no.7, pp. 1532- 1540, July (2002).
- [15] A. J. Prata and I. F. Grant, "Determination of mass loadings and plume heights of volcanic ash clouds from satellite data," *CSIRO Atmospheric Research and Technology Papers* **48**, 39, Commonwealth Science and Industry Research Organization, Melbourne, Victoria, Australia (2001).
- [16] B. Schölkopf and A. Smola, *Learning with kernels*. Cambridge, MA: MIT Press, (2002).
- [17] J. Shotton, M. Johnson, R. Cipolla, "Semantic texton forests for image categorization and segmentation," *IEEE Conf on Computer Vision and Pattern Recognition* 1–8 (2008).
- [18] D. R. Thompson, A. Allwood, D. Bekker, N. A. Cabrol, T. Estlin, T. Fuchs, K. L. Wagstaff, "TextureCam: Autonomous image analysis for astrobiology survey," *Lunar and Planetary Sciences Conference*, Houston, TX, (2012).
- [19] R. Wright, L. P. Flynn, H. Garbeil *et al.*, "MODVOLC: near-real-time thermal monitoring of global volcanism," *Journal of Volcanology and Geothermal Research*, *135*, 29-49 (2004).
- [20] Y. Yamaguchi, A. Kahle, H. Tsu *et al.*, "Overview of Advanced Spaceborne Thermal Emission and Reflection Radiometer (ASTER)," *IEEE Transactions on Geoscience and Remote Sensing*, *36*, 1062-1071(1998).